Formation and Sensing of Polyethyleneimine-Assisted Lyotropic Chromonic Liquid Crystal Droplets

Jun-Gang Li†, Zhao-Yan Yang†, Xing-Zhou Tang†, Zi-Jian Ou, Xiao-Hu Shang, Hao-Yi Jiang, Yan-Qing Lu, and Bing-Xiang Li

***Abstract*—Lyotropic chromonic liquid crystal (LCLC) droplets hold significant potential in both scientific research and practical applications. The incorporation of polyethyleneimine (PEI) and its impact on LCLC droplet formation present a compelling puzzle. This study reports the fabrication of micrometer-sized LCLC droplets through the self-assembly functionalization process by integrating cationic polymer PEI into a disodium cromoglycate (DSCG) solution. Notably, the droplet morphology can be reversibly altered between bipolar and radial configurations by modulating the pH of the surrounding aqueous solution, an effect attributable to the contraction of PEI chains. The findings indicate that the PEI-DSCG system can serve as a pH indicator in purified water and detect glucose concentrations as low as 0.1 mM by observing the ratio of bipolar to radial droplets under crossed polarizers. This investigation enhances the understanding of polymer-LCLC interactions and advances new avenues for developing pH-responsive systems and glucose-sensing technologies.**

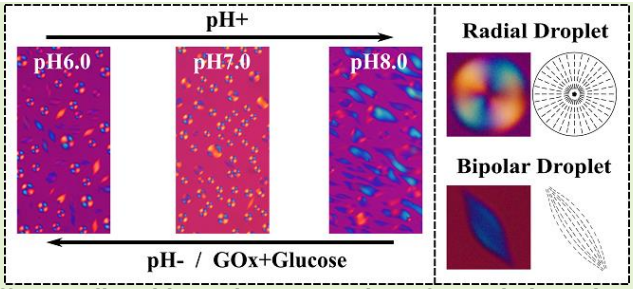

***Index Terms*—biosensor, droplet, glucose, lyotropic chromonic liquid crystal, pH**

†*These authors contributed equally to this work*

I. Introduction

Liquid crystals (LCs) are a unique state of matter that marries the fluidity of liquids with the order of crystalline solids, offering versatile applications in soft matter physics [1-4]. Among these, lyotropic chromonic liquid crystals (LCLCs), a specialized subclass of lyotropic liquid crystals (LLCs), have piqued scientific curiosity due to their distinctive molecular arrangement [5-14]. LCLCs, diverging from conventional LLCs, consist of discotic molecules featuring aromatic cores and ionic hydrophilic groups at their peripheries [15]. These molecules are known to self-assemble into columnar structures through non-covalent interactions, which are highly responsive to environmental factors like ionic presence [16] and temperature variations [17]. Such responsiveness is advantageous for applications in biological detection [18, 19], where disodium cromoglycate (DSCG), a well-studied LCLC, is notable for its biocompatibility and cost-effectiveness. Importantly, DSCG-based detection systems bypass the need for complex instrumentation, circumventing electrical interference commonly encountered in biological assays.

The detection of glucose, a vital biomolecule essential for metabolic functions, epitomizes the application of LCs in biomedical sensing. Normal blood glucose levels (BGL) in healthy individuals range from 3.9 to 7.8 mM, while levels surpassing 11 mM can precipitate hyperglycemia, leading to a spectrum of complications [20]. Given that the symptomatic manifestation of hyperglycemia often does not become apparent until BGL significantly elevates to 15-20 mM, there is a critical demand for vigilant glucose monitoring in medical diagnostics. Despite substantial advancements in glucose sensing technologies [21-23], challenges persist, notably the interference from ions and electric currents. Herein lies the potential of LC-based sensors, which are not only low-cost but also negate the necessity for external equipment, presenting a viable solution to current sensing limitations. For example, Dickert et al. used cholesteric liquid crystals to distinguish molecules according to their morphological properties [24].

Surfactants, particularly those with single-chain structures, are instrumental in forming stable water-in-oil vesicles by emulsifying oil-based substances, setting the stage for LC

This work is supported by the National Key Research and Development Program of China (No.2022YFA1405000), the National Natural Science Foundation of China (No. 62375141), the Natural Science Foundation of Jiangsu Province, Major Project (No. BK20212004),.and Natural Science Research Start-up Foundation of Recruiting Talents of Nanjing University of Posts and Telecommunications (No. NY222122, No. NY222105).

Bing-Xiang Li, Jun-gang Li, Zhao-Yan Yang, Xing-Zhou Tang, Zi-Jian Ou, Xiao-Hu Shang, and Hao-Yi Jiang are with Nanjing University of Posts and Telecommunications, College of Electronic and Optical Engineering & College of Flexible Electronics (Future Technology), Nanjing, 210023, China (e-mail: zyyang@njupt.edu.cn; bxli@njupt.edu.cn).

Bing-Xiang Li and Yan-Qing Lu are with the National Laboratory of Solid State Microstructures, College of Engineering and Applied Sciences, Nanjing University, Nanjing 210023, China. (e-mail: yqlu@nju.edu.cn)

applications. Research has shown that lipids [25] and surfactants [26] can prompt the self-assembly of LCs, resulting in the formation of micron-sized droplets [27-37]. In this work, we introduce a novel approach that utilizes cationic polymer polyethyleneimine (PEI) to catalyze the self-assembly of DSCG, forming radial LCLC droplets. This technique challenges the established notion that solely non-ionic or anionic water-soluble polymers are conducive to radial droplet formation in consort with water-solvated DSCG [29, 32, 33, 38]. We analyze how variations in PEI concentration and environmental pH impact droplet microstructure, revealing significant morphological changes under crossed polarizers upon pH alteration. Our findings demonstrate that the PEI-DSCG system is a promising candidate for glucose detection, as it utilizes pH-dependent morphological changes, enabling glucose concentration assessment with minimalistic setup and low cost, thus paving the way for innovative biosensing and biological material encapsulation methodologies.

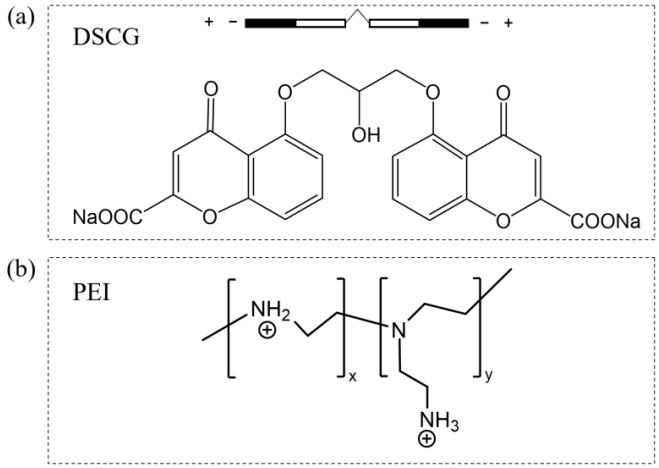

Fig. 1. The molecular structure of DSCG and PEI.

II. Experimental Materials and Methods

For all the experiments, we utilized disodium cromoglycate (DSCG, Sigma-Aldrich) and polyethyleneimine (PEI, Mw 10,000, Shanghai Titan Scientific), with their molecular structures depicted in Fig. 1. Disodium hydrogen phosphate (Na_2HPO4) and sodium dihydrogen phosphate (NaH_2PO4) were sourced from Sinopharm. We prepared buffer solutions of different pH by mixing Na_2HPO4 and NaH_2PO4 in varying volume ratios but maintaining consistent concentrations, as detailed in Table 1. Throughout our experiments, we used deionized (DI) water (Millipore Milli-Q grade) with a resistivity of 18.2 MΩ•cm.

The liquid crystal cells (LC cells) consisted of two parallel micro-slide glasses, with a calibrated thickness of 10 ± 1 μm, ensured by UV glue embedded with silicon particles. We prepared PEI aqueous solutions at varying concentrations: 1.0, 3.0, 4.8, 6.5, 9.1, 11.5, 13.0, and 15.0 wt%. DSCG was then dissolved in the PEI solutions to achieve final concentrations of 9.0 and 12.9 wt%. After a vortex reaction of approximately one minute, we heated the DSCG solution on a hot plate at 60°C before injecting it into the LC cell. The cells, with the DSCG sample enclosed, were subsequently sealed with epoxy glue to prevent water evaporation.

TABLE I
THE INGREDIENTS OF DIFFERENT PH BUFFER SOLUTIONS.

pH	0.2 M NaH_2PO_4 (mL)	0.2 M Na_2HPO_4 (mL)
7.1	0.660	1.340
7.2	0.560	1.440
7.3	0.460	1.540
7.4	0.380	1.620
7.5	0.320	1.680
7.6	0.260	1.740
7.7	0.210	1.790
7.8	0.170	1.830
7.9	0.140	1.860
8.0	0.106	1.894

To construct a phase diagram, we initially heated the DSCG samples to the isotropic phase on a hot plate (HCS402) and then allowed them to cool at a rate of 5°C/min using a temperature controller (mK2000B). We documented the results with a polarizing optical microscope (POM, Nikon ECLIPSE Ci-POL).

To assess the impact of pH, PEI was diluted with buffer solutions to a fixed concentration of 9.1 wt%. DSCG was dissolved in these PEI-enriched solutions at a concentration of 9.0 wt%. The samples were then cooled at a rate of 5°C/min .

For glucose detection, we combined a glucose solution with glucose oxidase (GOx) and placed drops on a micro-slide glass, maintaining the temperature at 40°C for ten minutes until dry. We then formed an LC cell by bonding the slide with a pre-cleaned glass. The glucose concentrations tested were 0.1, 0.5, 1.0, and 20 mM, with the GOx concentration at 0.01 wt%. We heated the mixture, containing 9.0 wt% DSCG and 9.1 wt% PEI at pH=7.8, to 70°C on a hot plate and injected it into the aforementioned cells at 55°C in the isotropic phase. The cells were sealed with epoxy resin to inhibit evaporation. Observations of the detection outcomes were conducted under a polarized optical microscope.

III. Results and Discussions

3.1 Analysis of PEI-Assisted DSCG Droplet Formation

The formation of droplets based on PEI-DSCG lyotropic chromonic liquid crystals is significantly influenced by the concentrations of DSCG and PEI. During the cooling phase, we first observed the emergence of bipolar droplets, characterized by two distinct sharp ends. Subsequently, these droplets underwent fusion and self-assembly, as depicted in Supplementary Movie 1. Radial droplets were prominently visible at a PEI concentration (C_{PEI}) of 9.1 wt%, as illustrated in Fig. 2 (a, b).

Our observations demonstrate an increase in the density of radial droplets (D_R) in tandem with the C_{PEI} , reaching a maximum of 9.1 wt% (Fig. 2c). However, further increases in C_{PEI} from 9.1 wt% to 13.0 wt% lead to a gradual decline in radial droplet density. Polarizing optical microscope (POM)

images of PEI-DSCG samples with a C_{PEI} of 13.0 wt% are presented in Supplementary Fig. S1, showing an almost complete absence of radial droplets. These findings indicate that the optimal C_{PEI} for generating PEI-assisted DSCG droplets is 9.1 wt%.

To analyze the microstructure of radial droplets, we define coordinate axes to describe their orientation and spatial arrangement. Herein, the x-axis aligns parallel to the polarizer, the y-axis is parallel to the analyzer, and the z-axis stands perpendicular to the LC cell surface. The droplets' projection on the x-y plane manifests as a symmetric circular structure. The cell thickness (d) limits the spatial expansion in the z-direction (Fig. 2d). When the cell thickness is reduced from 20 to 5 μm, the droplets show a clear four-petal structure, Fig. S2. Moreover, we have also examined the impact of the cooling rate. The findings suggest that as the cooling rate rises, the velocity of droplet fusion escalates, ultimately leading to the disruption of the radial morphology, Fig S3. Within each droplet, the director, denoting the LCLC molecules' orientation, is arranged radially and perpendicular to the Nematic-Isotropic (N-I) interface that demarcates the droplet from the surrounding solution. Prior studies have suggested that radial droplets are more stable than their tangential counterparts, attributed to the formation of robust hydrogen bonds [32, 33, 37]. Even after being subjected to ten rounds of thermal cycling, the PEI-DSCG droplets persist in maintaining their stability, as shown in Fig. S4. The enhanced stability of the droplets augurs well for biosensing applications, as it ensures the maintenance of structural integrity and functional properties, essential for reliable biosensing performance.

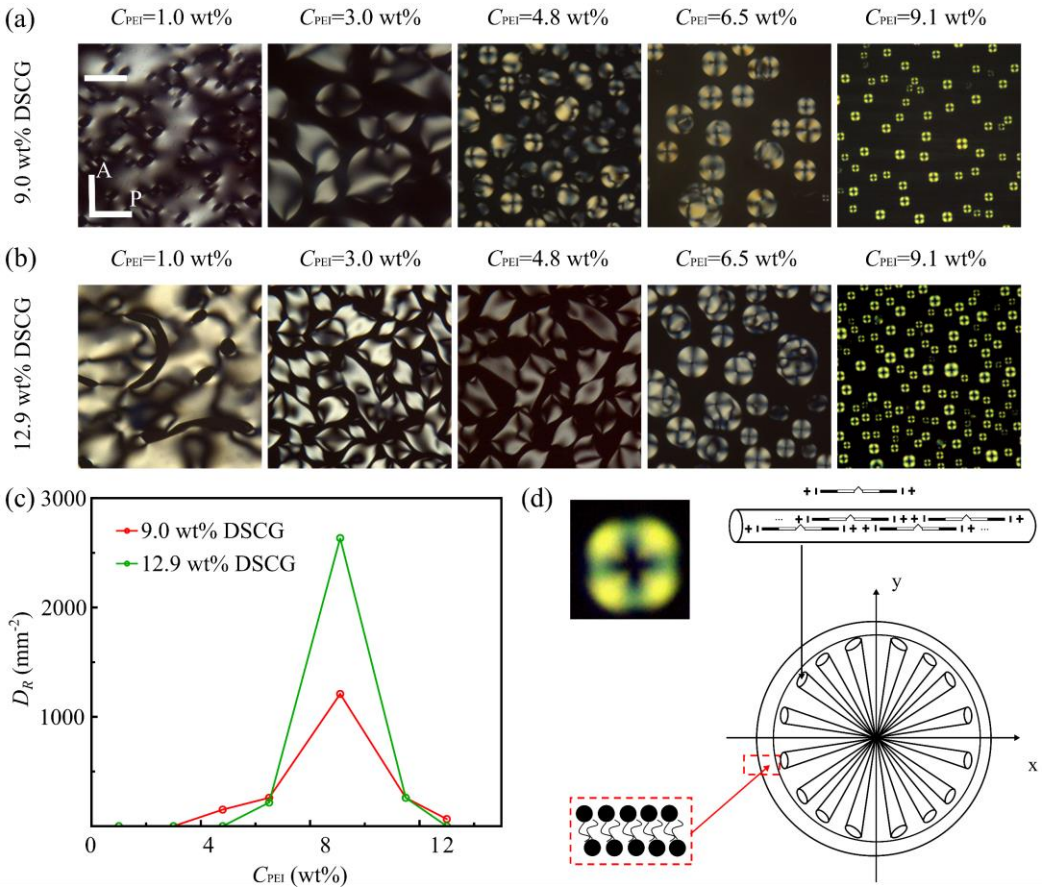

Fig. 2. Influence of C_{PEI} on PEI-DSCG droplet formation. POM images of (a) 9.0 wt% and (b) 12.9 wt% DSCG at different C_{PEI}; (c) The density of PEI-DSCG droplets varies with C_{PEI}; (d) Microstructure of a single droplet and orientation of the director. T=10°C. Scale bar 50 μm.

3.2 Analysis of pH Response in PEI-Assisted DSCG Droplet Formation

The role of pH within biological environments is pivotal. Therefore, we probed the pH-sensitive behaviors of PEI-DSCG droplets, recognizing from prior research that pH levels can modulate the adsorption and molecular ordering of PEI [39]. Our study identified three distinct steady states of droplets within varied pH contexts.

The first droplet type displayed a bipolar configuration with pronounced ends, maintaining a slender, smooth surface punctuated by a point defect at each extremity. Here, the director was situated along the line connecting these two defects. The second variant was the radial droplet, which presented radial symmetry akin to a sphere. An intermediary state was also observed, representing a transitional morphology between bipolar and radial forms, yielding an elliptical shape without the clear four-petal structure found in radial droplets, as seen in Fig. 3. In the cooling phase, bipolar droplets with pronounced ends were first to form, with some coalescing into annular structures

and others retaining their shape while expanding, as detailed in Supplementary Fig. S5. Upon heating, bipolar droplets were the first to vanish, with the director smoothing out near the point defects, signaling higher stability in circular droplets compared to bipolar ones.

Notably, with a pH increment from 6.0 to 7.0, the radial droplet density gradually increased, while that of bipolar droplets decreased. A marked transition in the PEI-DSCG system was evident at pH=6.0, suggesting that droplet morphology is markedly impacted by acidic conditions. As pH rose, the solution's charge density also increased, consolidating the stability of hydrogen bonds. This in turn altered interfacial tension, prompting radial droplets to evolve into bipolar ones, each maintaining symmetrical structures and highlighting a distinct coexistence state of both radial and bipolar droplets (R-B coexistence state).

Droplets in the PEI-DSCG system responded more noticeably to alkaline than acidic conditions within the pH range of 6.0 to 8.0. At pH=7.3, annular droplets transitioned extensively into bipolar or oval shapes, disrupting their symmetry. By pH=7.7, radial droplets were scarcely detectable, with bipolar droplets exhibiting evident distortion and bending. At pH=7.8, the prevalence of bipolar droplets diminished, eventually becoming imperceptible.

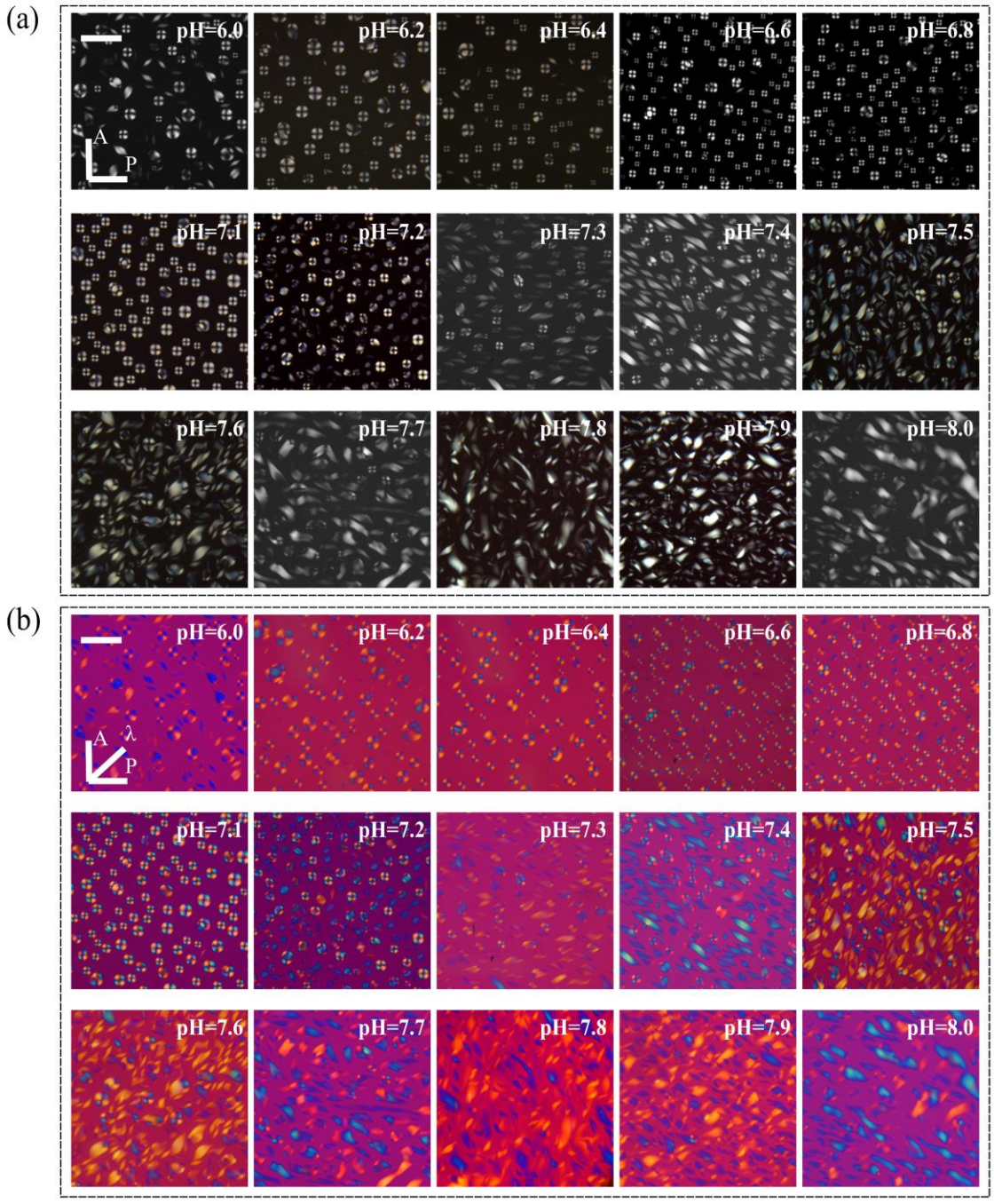

Fig. 3. POM images of PEI-DSCG droplets at different pH environments from 6.0 to 8.0. T=10℃. Scale bar 50 μm.

These outcomes suggest that droplet formation in alkaline conditions diverges from acidic ones. With pH elevation from 7.0 to 8.0, there was a surge in the population of both twisted radial and bipolar droplets. Concurrently, we observed the formation of intersecting bipolar structures, where droplets overlaid without merging, thus increasing overall density while reducing the average area.

Conversely, droplets in acidic environments were larger but fewer in number. From pH=7.0 down to 6.0, both radial and bipolar droplets coexisted, yet the symmetry of these formations persisted. This implies that environmental acidity impacts droplet size and frequency, meriting further investigative efforts to elucidate the precise mechanisms involved. However, environmental pH is instrumental in dictating droplet genesis and architecture.

Our analysis primarily addressed radial and bipolar droplets. Radial droplets displayed a symmetrical orientation with a central point defect, while bipolar droplets bore two sharp ends with directors aligned accordingly, as depicted in Fig. 4a. Observations showed the relative density (D_R/D) of radial and bipolar droplets shifted with pH levels, as outlined in Fig. 4b. At around pH=7, radial droplets peaked, denoting their abundance, while the growth rate of bipolar droplets was notably more rapid in alkaline environments. These variable proportions of droplet types offer a potential standard for pH assessment. Furthermore, the trend of decreasing average droplet area ($\bar{S}$) with rising pH suggests inhibited droplet fusion under more alkaline conditions, as possibly evidenced in Fig. 4c. The temperature decline led to a swift rise and then a gradual fall in droplet density, with acidic solutions yielding lower densities compared to alkaline ones, as shown in Fig. 4d. In a word, although the proportion of droplets appears similar in alkaline and acidic solutions, there are distinct differences in properties such as symmetry and density. These findings underscore the pronounced sensitivity of PEI-DSCG droplets to pH variations.

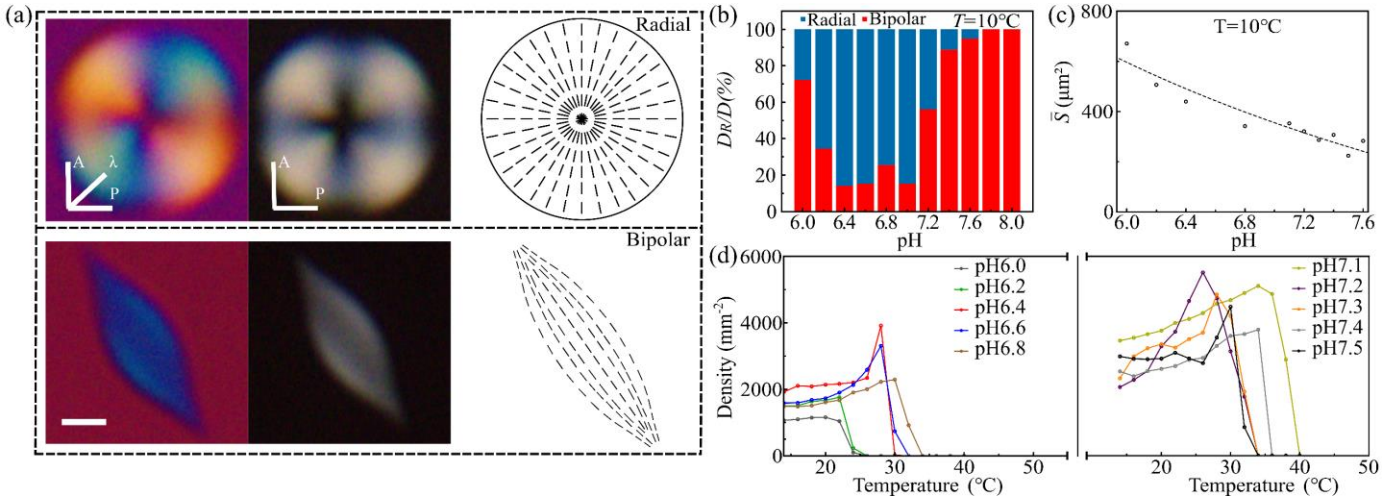

Fig. 4. (a) The director orientation of radial and bipolar droplets; (b) The proportion of the radial and bipolar droplets at different pH values; (c) The change of average area about radial droplets at different pH values; The density of PEI-DSCG droplet at (d) the acidic environment and the alkaline environment. Scale bar 4 μm .

This analysis delves into the behavior of droplets under distinct environmental conditions, focusing on their responses in alkaline and acidic contexts. Prior research has shed light on how changes in droplet morphology and behavior correlate with interfacial tension among other factors. Citing K. A. Simon et al. [33], it is suggested that droplets evolve from spherical to various other shapes under conditions of low interfacial tension. Conversely, P. Prinsen et al. have posited that a spherical droplet morphs into an elongated bipolar form when the dimensionless ratio:

$$\kappa \equiv K / \tau V^{1/3} \quad (1)$$

surpasses approximately unity [40]. In this formula, K represents a Frank elastic constant, τ is the interfacial tension between coexisting phases, and V denotes the droplet volume.

In light of these findings, we postulated that an alkaline environment intensifies the electrostatic repulsion between adjacent droplets, leading to the contraction of PEI chains. As a result, droplets elongate narrowly and lengthwise, aiming to minimize surface energy. In contrast, acidic conditions exert a milder impact on droplets, predominantly bolstering the stability of hydrogen bonds and diminishing interfacial tension without causing PEI chains to contract. Consequently, this fosters the transition of radial to bipolar droplets without markedly influencing their fusion and symmetry. Therefore, droplets in an alkaline milieu exhibit a disordered radial-bipolar (R-B) coexistence state, whereas those in an acidic setting tend to display a more orderly R-B coexistence state.

3.3 pH Detection of Purified Water

Wang et al. fabricated carbon dots to detect mineral water pH from 6.0 to 9.0 [41]. Taking inspiration from this concept, we tested the pH value of four types of purified water with different brands: Nongfu Spring, Cestbon, Ganten, and ALKAQUA (denoted as brands A to D) based on the pH-responsive property of PEI-DSCG droplets. The proportion of radial droplets in different solutions is calculated and displayed in Fig. 5. POM images of brands A to D are shown in Supplementary Fig. S6

(a-d). The results reveal that the droplet proportion of brands A, B, C, and D is close to the situation of pH=7.4, pH=7.2, pH=7.3, and pH=7.1, respectively. This indicates that the pH value of different types of purified water can be deduced by PEI-DSCG droplets. The results vividly demonstrate that PEI-DSCG droplets have a huge potential for pH detection even at low-ion concentrations.

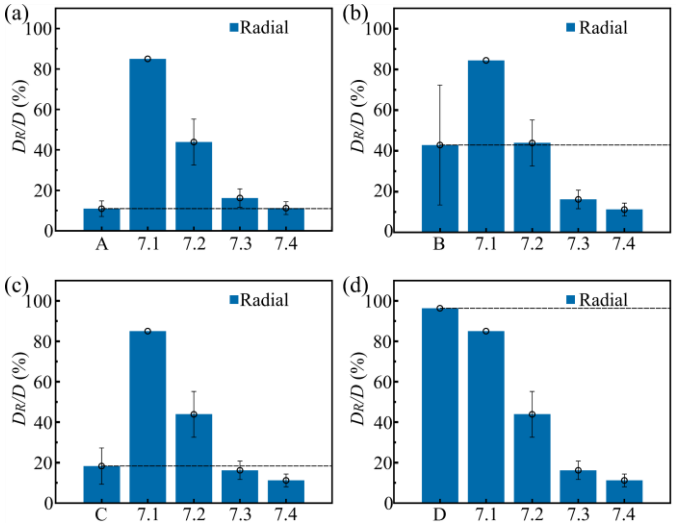

Fig. 5. pH detection of purified water. The proportion of radial droplets in (a) brand A, (b) brand B, (c) brand C, and (d) brand D.

3.4 Glucose Detection of PEI-Assisted Droplet

Our pH-responsive glucose detection approach leverages the sensitivity of PEI-DSCG droplets to changes in alkalinity. The detection mechanism is depicted in Fig. 6. The addition of glucose oxidase (GOx) to the solution triggers the oxidation of glucose into gluconate, culminating in a reduction of the solution's pH. Consequently, within PEI-DSCG solutions at pH=7.8, bipolar droplets transition into radial droplets, a process designated as the B-R transformation. By assessing the ratio of radial droplets, we can determine varying glucose concentrations.

Fig. 7 (a, b) exhibits the detection outcomes for 20 mM glucose solutions. Sequential images show the polarized optical microscopy (POM) visuals of glucose alone, the combination of glucose with GOx, and GOx alone in PEI-DSCG solutions. These observations confirm that neither glucose nor GOx alone prompts alterations in droplet structure in comparison to the baseline PEI-DSCG aqueous solution at pH=7.8. However, a substantial shift in droplet morphology occurs when glucose and GOx are mixed, verifying that the B-R transformation is prompted by the byproducts of glucose's oxidative reaction.

To ascertain the specificity of this method, we also detected fructose, another monosaccharide, as shown in Fig. 7 (c, d). The absence of the B-R transformation, even in the presence of fructose and GOx under identical conditions, suggests that PEI-DSCG droplets are selective for glucose.

In sum, our method illustrates the capacity of PEI-DSCG droplets to detect glucose via a pH-dependent B-R transformation, induced by glucose oxidation byproducts. The lack of transformation with fructose underscores the method's specificity.

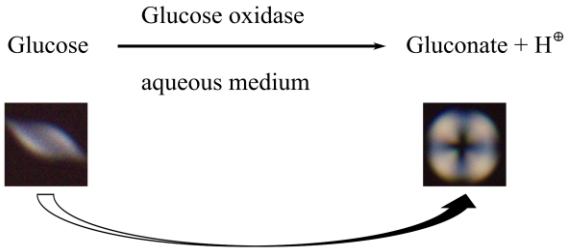

Fig. 6. GOx-Catalyzed Oxidation of Glucose.

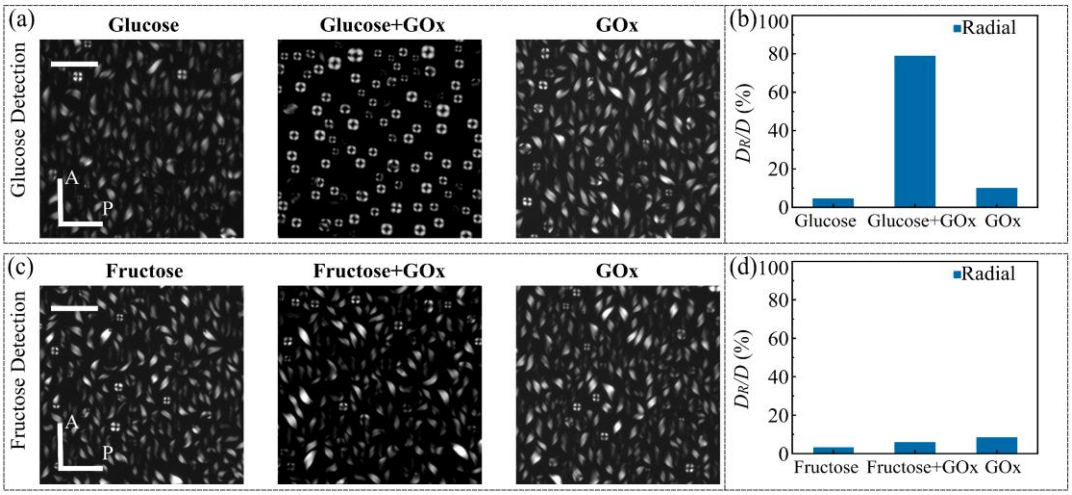

Fig. 7. Glucose detection based on PEI-DSCG droplets. POM images of PEI-DSCG solution for (a) 20 mM glucose detection and (c) 20 mM fructose detection. (Left to right: glucose or fructose existed alone, glucose or fructose mixed GOx, and GOx existed alone); The proportion of radial droplets in (b) glucose detection and (d) fructose detection. Scale bar 50 μm .

We further examined how glucose concentration affects the proportion of radial droplets. For this sensitivity assessment, we chose an optimal glucose solution volume of 120 μL . At this volume, over half of the bipolar droplets shifted to radial

droplets, marking a pronounced B-R transformation, as depicted in Fig. 8a. Fig. 8b presents the percentage of radial PEI-DSCG droplets at varying glucose concentrations (0.1, 0.5, and 1 mM). A noticeable B-R transformation was observed even with a 0.1 mM glucose solution, indicating that our detection method can discern glucose concentrations as low as 0.1 mM.

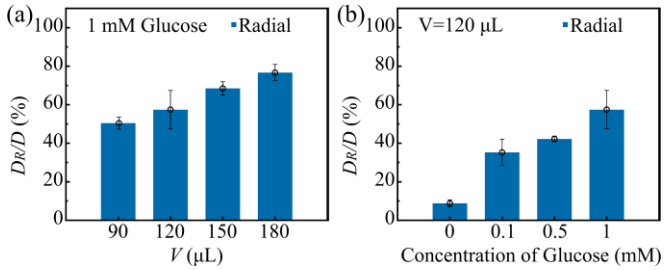

Fig. 8. The relationship between the proportion of radial droplets and (a) the volume of the solution dropped on the micro-slide glass, and (b) the concentration of glucose.

IV. Conclusions

This investigation confirms that the cationic polymer PEI, in conjunction with DSCG, is capable of forming radial droplets. We have observed both the formation process and the proportions of droplets, enabling precise pH detection within the solution. Moreover, this methodology allows for the detection of pH in purified water and the presence of glucose at concentrations as minute as 0.1 mM. This advancement broadens our comprehension of the polymer-DSCG interplay and introduces novel prospects for pH-reactive mechanisms and glucose monitoring. LC droplets are engendered by the coating of single-chain surfactants on their surfaces, with the droplet morphology being governed by the liquid crystal characteristics and the nature of hydrogen bonding. Although thermotropic LC droplets, such as those of 5CB, have been employed in detecting various biological substances [34-36], their formation typically necessitates intricate microfluidic channels and extended periods, coupled with their intrinsic biological toxicity, limiting their biological applications. In contrast, the PEI-DSCG droplets discussed herein offer promising utilities in diverse biological settings, including blood, owing to their biocompatibility, straightforward production, cost-effectiveness, and high fidelity. These attributes render them exceptionally suited for bio-sensing applications that are both efficient and facile.

References

[1] Y. Huang, Y. Xu, H. K. Bisoyi *et al.*, "Photocontrollable Elongation Actuation of Liquid Crystal Elastomer Films with Well-Defined Crease Structures," *Adv. Mater.,* vol. 35, no. 36, pp. 2304378, 2023.

[2] R. Zheng, L. Ma, W. Feng *et al.*, "Autonomous Self-Sustained Liquid Crystal Actuators Enabling Active Photonic Applications," *Adv. Funct. Mater.,* pp. 2301142, 2023.

[3] J. Jiang, X. Wang, O. I. Akomolafe *et al.*, "Collective transport and reconfigurable assembly of nematic colloids by light-driven cooperative molecular reorientations," *Proc. Natl. Acad. Sci. U.S.A.,* vol. 120, no. 16, pp. e2221718120, 2023.

[4] C. Peng, T. Turiv, Y. Guo *et al.*, "Control of colloidal placement by modulated molecular orientation in nematic cells," *Sci. adv.,* vol. 2, no. 9, pp. e1600932, 2016.

[5] Lin, Bao-Ping, Sun *et al.*, "Novel crosslinked lyotropic liquid crystal materials based on acrylate-type gemini ammonium surfactant," *Liq. Cryst.,* vol. 42, no. 4, pp. 520-529, 2015.

[6] D. Liu, Y. Chang, D. Tian *et al.*, "Lyotropic liquid crystal self-assembly of H2O2-hydrolyzed chitin nanocrystals," *Carbohydr. Polym.,* vol. 196, pp. 66-72, 2018.

[7] X. Feng, Q. Imran, Y. Zhang *et al.*, "Precise nanofiltration in a fouling-resistant self-assembled membrane with water-continuous transport pathways," *Sci. adv.,* vol. 5, no. 8, pp. eaav9308, 2019.

[8] C. Peng, Y. Guo, T. Turiv *et al.*, "Patterning of Lyotropic Chromonic Liquid Crystals by Photoalignment with Photonic Metamasks," *Adv. Mater.,* vol. 29, no. 21, pp. 1606112, 2017.

[9] S. Zhou, S. V. Shiyanovskii, H. S. Park *et al.*, "Fine structure of the topological defect cores studied for disclinations in lyotropic chromonic liquid crystals," *Nat. Commun.,* vol. 8, pp. 14974, 2017.

[10] R. Koizumi, D. Golovaty, A. Alqarni *et al.*, "Toroidal nuclei of columnar lyotropic chromonic liquid crystals coexisting with an isotropic phase," *Soft Matter,* vol. 18, no. 38, pp. 7258-7268, 2022.

[11] "Periodic Arrays of Chiral Domains Generated from the Self-Assembly of Micropatterned Achiral Lyotropic Chromonic Liquid Crystal," *ACS Cent. Sci.,* vol. 6, no. 11, pp. 1964-1970, 2020.

[12] H. S. Yun, G. Park, and D. K. Yoon, "Orientation control of lyotropic chromonic liquid crystals in the capillary bridge," *J. Mater. Chem. C,* vol. 10, no. 17, pp. 6878-6884, 2022.

[13] Y. J. Cha, M. J. Gim, H. Ahn *et al.*, "Orthogonal Liquid Crystal Alignment Layer: Templating Speed-Dependent Orientation of Chromonic Liquid Crystals," *ACS Appl. Mater. Interfaces,* vol. 9, no. 21, pp. 18355-18361, 2017.

[14] C. Peng, and O. Lavrentovich, "Chirality Amplification in Tactoids of Lyotropic Chromonic Liquid Crystals," *Soft Matter,* vol. 2014, pp. G18. 013, 2014.

[15] Y. Guo, H. Shahsavan, Z. S. Davidson *et al.*, "Precise control of lyotropic chromonic liquid crystal alignment through surface topography," *ACS Appl. Mater. Interfaces,* vol. 11, no. 39, pp. 36110-36117, 2019.

[16] S. Zhou, "Recent progresses in lyotropic chromonic liquid crystal research: elasticity, viscosity, defect structures, and living liquid crystals," *Liq. Cryst. Today,* vol. 27, no. 4, pp. 91-108, 2018.

[17] T. Ogolla, R. S. Paley, and P. J. Collings, "Temperature dependence of the pitch in chiral lyotropic chromonic liquid crystals," *Soft Matter,* vol. 15, no. 1, pp. 109-115, 2019.

[18] E. Otón, J. M. Otón, M. Cao-García *et al.*, "Rapid detection of pathogens using lyotropic liquid crystals," *Opt. Express,* vol. 27, no. 7, pp. 10098, 2019.

[19] S. V. Shiyanovskii, T. Schneider, I. I. Smalyukh *et al.*, "Real-time microbe detection based on director distortions around growing immune complexes in lyotropic chromonic liquid crystals," *Phys. Rev. E.,* vol. 71, no. 2, pp. 020702, 2005.

[20] D. Giugliano, R. Marfella, L. Coppola *et al.*, "Vascular effects of acute hyperglycemia in humans are reversed by L-arginine: evidence for reduced availability of nitric oxide during hyperglycemia," *Circulation,* vol. 95, no. 7, pp. 1783-1790, 1997.

[21] E. S. Forzani, H. Q. Zhang, L. A. Nagahara *et al.*, "A conducting polymer nanojunction sensor for glucose detection," *Nano Lett.,* vol. 4, no. 9, pp. 1785-1788, 2004.

[22] Y. H. Lin, F. Lu, Y. Tu *et al.*, "Glucose biosensors based on carbon nanotube nanoelectrode ensembles," *Nano Lett.,* vol. 4, no. 2, pp. 191-195, 2004.

[23] J. Wang, J. W. Mo, S. F. Li *et al.*, "Comparison of oxygren-rich and mediator-based glucose-oxidase carbon-paste electrodes," *Anal. Chim. Acta,* vol. 441, no. 2, pp. 183-189, 2001.

[24] F. L. Dickert, A. Haunschild, P. Hofmann *et al.*, "Molecular recognition of organic solvents and ammonia: shapes and donor properties as sensor effects," *Sens. Actuators, B,* vol. 6, no. 1-3, pp. 25-28, 1992.

[25] J. Zhai, C. Fong, N. Tran *et al.*, "Non-Lamellar Lyotropic Liquid Crystalline Lipid Nanoparticles for the Next Generation of Nanomedicine," *ACS Nano,* vol. 13, no. 6, pp. 6178-6206, 2019.

[26] K. Steck, S. Dieterich, C. Stubenrauch *et al.*, "Surfactant-based lyotropic liquid crystal gels-the interplay between anisotropic order and gel formation," *J. Mater. Chem. C,* vol. 8, no. 16, pp. 5335-5348, 2020.

[27] J. Fan, Y. Li, H. K. Bisoyi *et al.*, "Light-Directing Omnidirectional Circularly Polarized Reflection from Liquid-Crystal Droplets," *Angew. Chem. Int. Ed.,* vol. 127, no. 7, pp. 2188-2192, 2014.

[28] L. Chen, Y. Li, J. Fan *et al.*, "Photoresponsive Monodisperse Cholesteric Liquid Crystalline Microshells for Tunable Omnidirectional Lasing Enabled by a Visible Light-Driven Chiral Molecular Switch," *Adv. Opt. Mater.,* vol. 2, no. 9, pp. 904-904, 2014.

[29] N. Varghese, G. S. Shetye, D. Bandyopadhyay *et al.*, "Emulsion of aqueous-based nonspherical droplets in aqueous solutions by single-chain surfactants: templated assembly by nonamphiphilic lyotropic liquid crystals in water," *Langmuir,* vol. 28, no. 29, pp. 10797-807, 2012.
[30] R. Koizumi, B. X. Li, and O. D. Lavrentovich, "Effect of Crowding Agent Polyethylene Glycol on Lyotropic Chromonic Liquid Crystal Phases of Disodium Cromoglycate," *Crystals,* vol. 9, no. 3, pp. 160, 2019.
[31] M. Rajabi, H. Baza, T. Turiv *et al.*, "Directional self-locomotion of active droplets enabled by nematic environment," *Nat. Phys.,* vol. 17, no. 2, pp. 260-266, 2021.
[32] R. Koizumi, D. Golovaty, A. Alqarni *et al.*, "Topological transformations of a nematic drop," *Sci. Adv.,* vol. 9, no. 27, pp. eadf3385, 2023.
[33] K. A. Simon, P. Sejwal, R. B. Gerecht *et al.*, "Water-in-water emulsions stabilized by non-amphiphilic interactions: polymer-dispersed lyotropic liquid crystals," *Langmuir,* vol. 23, no. 3, pp. 1453-1458, 2007.
[34] J. Kim, M. Khan, S. Y. Park *et al.*, "Glucose sensor using liquid-crystal droplets made by microfluidics," *ACS Appl. Mater. Interfaces,* vol. 5, no. 24, pp. 13135-13139, 2013.
[35] Y. D. Jung, M. Khan, and S. Y. Park, "Fabrication of temperature- and pH-sensitive liquid-crystal droplets with PNIPAM-b-LCP and SDS coatings by microfluidics," *J. Mater. Chem. B,* vol. 2, no. 30, pp. 4922-4928, 2014.
[36] Y. Wang, L. Zhao, A. Xu *et al.*, "Detecting enzymatic reactions in penicillinase via liquid crystal microdroplet-based pH sensor," *Sens. Actuators, B,* vol. 258, pp. 1090-1098, 2018.
[37] K. A. Simon, P. Sejwal, E. R. Falcone *et al.*, "Noncovalent polymerization and assembly in water promoted by thermodynamic incompatibility," *J. Phys. Chem. B,* vol. 114, no. 32, pp. 10357-10367, 2010.
[38] L. Tortora, H. S. Park, S. W. Kang *et al.*, "Self-assembly, condensation, and order in aqueous lyotropic chromonic liquid crystals crowded with additives," *Soft Matter,* vol. 6, no. 17, pp. 4157-4167, 2010.
[39] E. Tran, A. P. Carpenter, and G. L. Richmond, "Probing the Molecular Structure of Coadsorbed Polyethylenimine and Charged Surfactants at the Nanoemulsion Droplet Surface," *Langmuir,* vol. 36, no. 31, pp. 9081-9089, 2020.
[40] P. Prinsen, and V. D. S. Paul, "Shape and director-field transformation of tactoids," *Phys. Rev. E.,* vol. 68, no. 2, pp. 021701, 2003.
[41] T. Wang, G. Chen, L. Li *et al.*, "Highly Fluorescent Green Carbon Dots as a Fluorescent Probe for Detecting Mineral Water pH," *Sensors,* vol. 19, no. 17, pp. 3801, 2019.

Jun-Gang Li is currently pursuing his M.S. degree in the major of optical engineering at Nanjing University of Posts and Telecommunications, Nanjing, China. His research interests include the regulation of lyotropic liquid crystals doped with compounds and biological applications.

Zhao-Yan Yang is a Lecturer at Nanjing University of Posts and Telecommunications. She graduated from School of electronic science and engineering in Southeast University and received the Ph.D. degree in Optical Engineering in 2022. Her research interests focus on biosensing and bioimaging of lyotropic liquid crystals and functional nanomaterials.

Xing-Zhou Tang received his Ph.D. degree in Physics from Advanced Material and Liquid Crystal Institute & Department of Physics at Kent State University USA in 2020. He is currently a professor at Nanjing University of Posts and Telecommunications. He is deeply engaged in exploring the mechanisms and topological properties of liquid crystals, focusing on unraveling their intricate behaviors and applications.

Zi-Jian Ou is currently pursuing his M.S. degree in the major of optical engineering at Nanjing University of Posts and Telecommunications, Nanjing, China. His research interests are the orientation and biological applications of lyotropic liquid crystals.

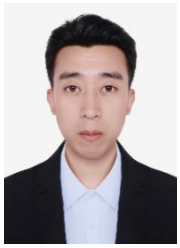

Xiao-Hu Shang is currently pursuing his M.S. degree in the major of optical engineering at Nanjing University of Posts and Telecommunications, Nanjing, China. His research interests are electro-optic regulation and pattern formation of liquid crystals.

Hao-Yi Jiang is currently working toward his Ph.D. degree in electronic science and technology at Nanjing University of Posts and Telecommunications, Nanjing, China. His research interests include the biological detection of liquid crystals and the application of lyotropic liquid crystals.

Yan-Qing Lu received his Ph.D. degree from Nanjing University, China, in 1996. He is currently a Changjiang Distinguished Professor at Nanjing University and a Fellow of the Optical Society of America and Chinese Optical Society. His research interests include liquid crystal photonics, fiber optics, and nonlinear optics.

Bing-Xiang Li received his Ph.D. degree in Chemical Physics from Advanced Material and Liquid Crystal Institute at Kent State University USA in 2019. He is currently a Professor at Nanjing University of Posts and Telecommunications. His current research spans from liquid crystals, stimuli-responsive soft matter, and active matter, to biological physics.